Matrix approximations of operators

B. G. Giraud^{1*}, S. Karataglidis^{2,3†}, K. Murulane^{2‡}, R. Peschanski^{1#}

¹Institut de Physique Théorique, Centre d'Etudes,

CEA-Saclay, 91191 Gif-sur-Yvette, France

²Department of Physics, University of Johannesburg,

P.O. Box 524, Auckland Park, 2006, South Africa

³School of Physics, The University of Melbourne, Victoria, 3010, Australia

(*#robi.peschanski@ipht.fr)

(*‡kmurulane@uj.ac.za)

(*†stevenka@uj.ac.za)

(**bertrand.giraud@ipht.fr)

(Dated: November 26, 2025)

Abstract

The approximate representation of operators by finite matrices is analysed in terms of accuracy and convergence. The identity operator, for example, can be reconstructed using a basis of harmonic oscillator states leading to a narrow peak approximation of the δ function, but this peak may be perturbed by small, residual, oscillations. The peak does not shrink nor grows quickly, and the oscillations only diminish slowly as the size of the matrix increases. For the kinetic energy operator, a triple peak (one positive, two negative) representation of $-\delta''$ is obtained, but that is affected also by residual oscillations. Again, convergence is slow as the matrix dimension increases. We find compact formulas to explain such oscillations. Similar observations are found for representations of local interactions, while separable potentials are better represented. As a comparison, in the context of a toy model, the effects of choosing an alternative single particle basis are studied. A formal approach [1] for the approximation of operators is considered for comparison. We conclude with a word of caution for (finite) matrix approximations of operators.

I. INTRODUCTION AND BASIC FORMALISM

There are many instances in physics where one makes use of operators that have simple representations in either coordinate or momentum space [2–5]. We wish to consider representations of such operators, whose eigenstates may span an infinite dimensional space, as finite matrices, where that restriction is forced by the need to diagonalise the Hamiltonian of a system. We will consider the case of a system of A identical particles whose Hamiltonian is H = T + V, where $T = \sum_{i=1}^{A} p_i^2/(2m)$ is the kinetic energy and $V = \sum_{i < j} v (|\mathbf{r}_i - \mathbf{r}_j|) + v_{cm}$ is the potential. Therein, v is a two-body potential, which is often invariant under rotations and also local, although non-local, and separable in particular, potentials have sometimes been used. The elementary mass is m, while $\mathbf{p}_i \equiv \{p_{xi}, p_{yi}, p_{zi}\}$ and $\mathbf{r}_i \equiv \{x, y, z\}$ are the momentum and position of particle i, respectively. The center-of-mass (cm) potential is $v_{cm} = Am\omega^2 R^2/2$, where $\mathbf{R} \equiv \{X, Y, Z\} = A^{-1} \sum_{i=1}^{A} \mathbf{r}_i$ factorises the cm in a spherical Gaussian packet at the origin of the laboratory frame, with energy $\frac{3}{2}\hbar\omega$. This serves to remove translational degeneracy. Without such a term, which is frequently omitted in the literature, the ground state of H would not be square integrable as the omission leads to a zero momentum plane wave for the system's cm.

Because T and V do not commute, there are very few cases where the diagonalisation of H, by the solution of (integro)-differential equations, is analytically or numerically viable. Approximations, leading to linear or nonlinear formulations, are necessary. The most familiar approximation is that of projecting H onto a finite dimensional subspace spanned by a set of "basis states" $|i\rangle$, and diagonalising the finite matrix made by the matrix elements, $H_{ij} \equiv \langle i | H | j \rangle$, i, j = 1, ..., N, where the basis is truncated at N states. The truncated basis may span a complete enough space but that is not usually the case. Indeed, it has been shown that when such a truncated basis cannot span the complete space, a convergence problem exists [1] in the search of the solution to the Hamiltonian. One expects that with larger N generating larger embedded subspaces, there would be convergence to the full space. The motivation of this work is to examine such truncations with actual Hamiltonians and how a finite set of matrix elements H_{ij} might converge to the full H or not.

The first choice to be made in this study is the choice of expansion functions. Given a regular local v(r), the totality of suitably normalised eigenstates $\varphi(r)$ of a one-dimensional, one-body Hamiltonian, $h = -d^2/dr^2 + v(r)$, which may be either discrete or continuous,

provides a resolution of the identity operator [6], viz.

$$\delta(r-s) = \sum_{n} \varphi_{n}(r) \varphi_{n}^{*}(s) + \int d\varepsilon \, \varphi_{\varepsilon}(r) \, \varphi_{\varepsilon}^{*}(s) \,. \tag{1}$$

This kind of expansion extends to multidimensional and multiparticle problems by means of tensor algebra. It can also include resonant states and coupled channels [7]. As a first choice, and for simplicity, we use the (one-dimensional) harmonic oscillator basis,

$$\varphi_{1}(r) = \pi^{-1/4} e^{-r^{2}/2}
\varphi_{2}(r) = \sqrt{2}\pi^{-1/4} e^{-r^{2}/2}
\varphi_{3}(r) = \frac{\pi^{-1/4} (2r^{2} - 1)}{\sqrt{2}} e^{-r^{2}/2}
\vdots$$
(2)

as the set of expansion functions. In Section V, we extend the formalism beyond this simple basis.

In Section II, we analyse how the identity operator is approximated by finite rank kernels. A similar analysis is performed for the kinetic energy operator in Section III while local and separable potentials are considered in Section IV. The analyses are reconsidered in Section V when switching to an alternative expansion set of states. The basis is adjusted to a symmetry of the problem in Section VI and the results are discussed with regards to the inclusion of the symmetry. Section VII considers an alternative approach based on projection operators to split the Hilbert space into two or three subspaces. We conclude in Section VIII, comparing both approaches. An Appendix describes compact formulas representing matrix expansions of elementary operators onto harmonic oscillator wave functions.

II. THE IDENTITY OPERATOR IN TERMS OF THE EXPANSION BASIS

We begin by calculating the kernels

$$D_N(r,s) = \sum_{i=1}^{N} \varphi_i(r) \varphi_i(s).$$
(3)

The kernel in Eq. (3) is invariant under exchange of r and s and when both r and s change sign. These kernels should approximate the function $\delta(r-s)$ and the aim is to assess the convergence of the function in Eq. (3) to the δ function.

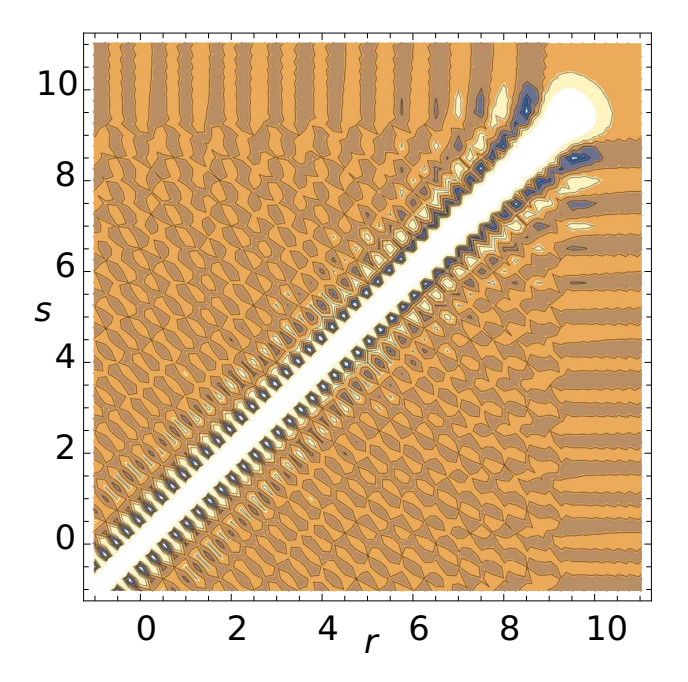


FIG. 1. Contour plot of the "approximate δ -function" $D_N\left(r,s\right)$ obtained with N=50 harmonic oscillator components.

The expansion basis used in Eq. (3) is that of a set of harmonic oscillator states which themselves are functions of Hermite polynomials, with the basis truncated to N states. The restriction to N states provides at most estimates of the mean square radii, $\sqrt{r^2}$ and $\sqrt{s^2}$, which themselves are of order \sqrt{N} . Any results obtained therefrom for $D_N(r,s)$ should only be considered if |r| and |s| are confined to a box of size, say $1.5\sqrt{N}$ at most.

Figure 1 is a contour plot of $D_{50}(r,s)$. A ridge pattern is clearly observed along the oblique axis defined by r=s. As expected from the root mean square radius argument above, this ridge strongly lowers as soon as $r=s\approx 7$. It exponentially decays beyond $r=s\approx 10$.

Figure 2 shows the crest profile, $D_{50}(r,r)$, of this ridge, from which we may make two observations. The more important one is that the profile's global trend is of a decreasing, curved line, inducing a non negligible variation of the quality of the simulation of the δ -function, while a plateau in some range would have hinted a partly stable quality. When N = 200, as shown in Fig. 3, one also does not observe such a plateau.

The second observation is the roughness of the crest. Small, but visible oscillations are

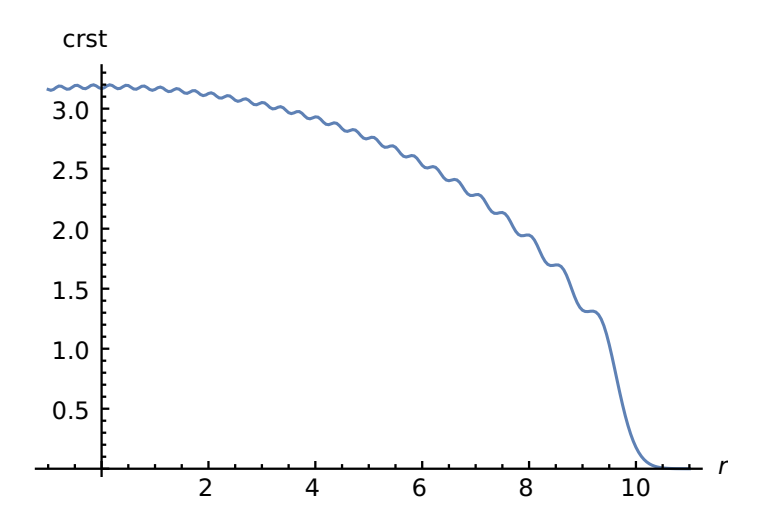


FIG. 2. Crest profile $D_{50}\left(r,r\right)$ of the ridge in Fig. 1.

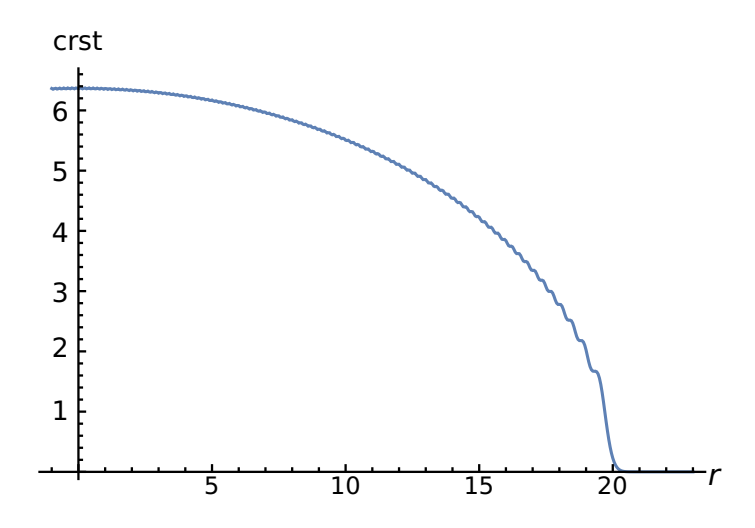


FIG. 3. As for Fig. 2 but for N = 200.

found when N = 50, indicating a lack of full convergence. For N = 200, they become much smaller but remain. The nature of the oscillations is clarified by the Christoffel-Darboux formula Eq. (A2), a general property for orthogonal polynomials [8] (see the Appendix for generalisations),

$$D_{N}(r,s) = \frac{1}{s-r} \sqrt{\frac{N}{2}} \left[\varphi_{N+1}(s) \varphi_{N}(r) - \varphi_{N+1}(r) \varphi_{N}(s) \right]. \tag{4}$$

Figures 4 and 5 portray the cuts of the N=50 ridge at s=0 and s=3, respectively. The

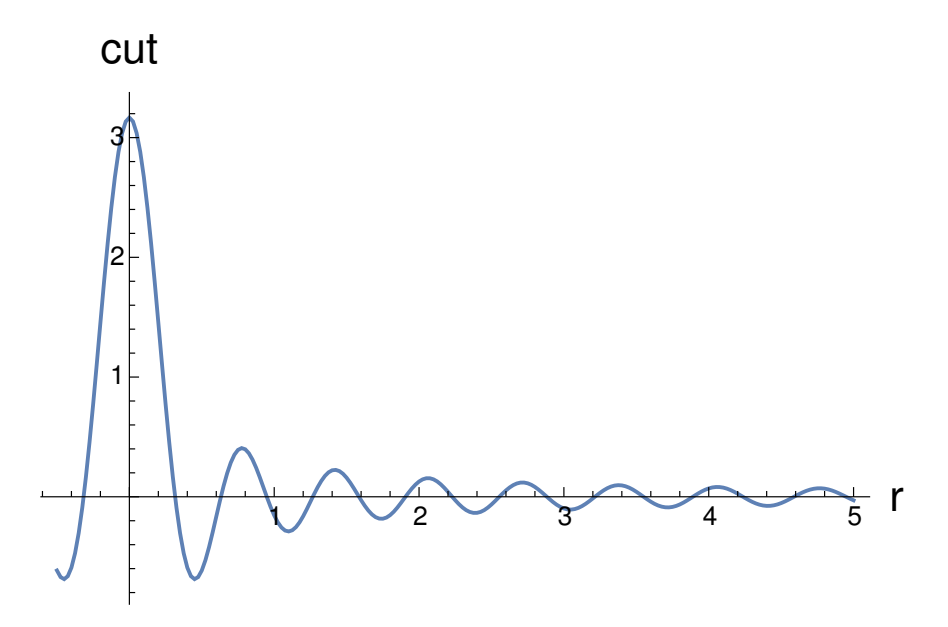


FIG. 4. Shape $D_{50}\left(r,0\right)$ of the s=0 cut of the ridge when N=50.

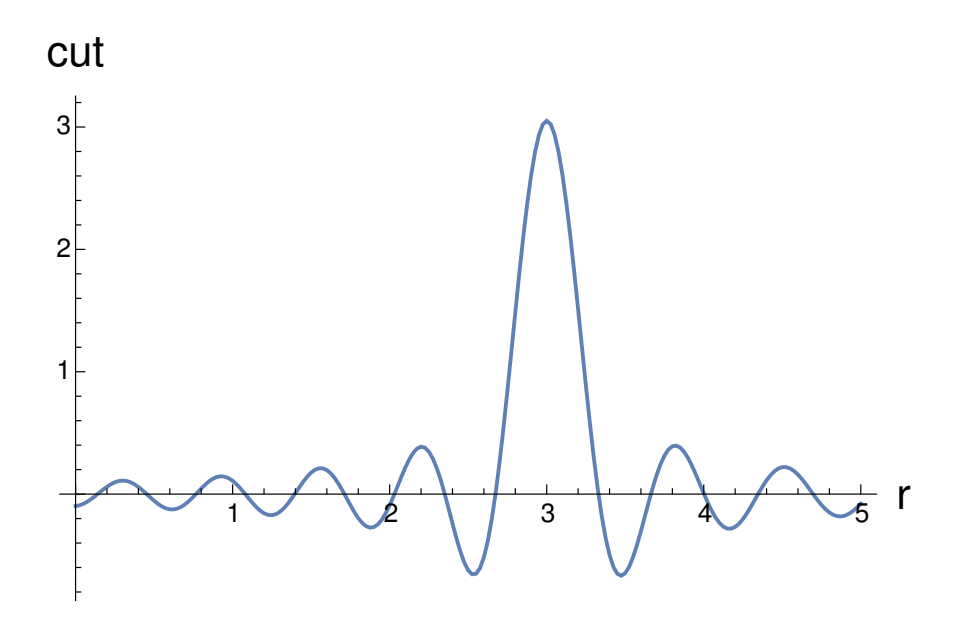


FIG. 5. Shape $D_{50}\left(r,3\right)$ of the s=3 cut of the same ridge.

shapes, $D_{50}(r, 0)$ and $D_{50}(r, 3)$, appear as approximations of δ functions centered at r = 0 and r = 3, respectively. They do show properly centered, somewhat high, and somewhat narrow peaks. But they are plagued by their oscillating tails, the influence of which may be non-negligible.

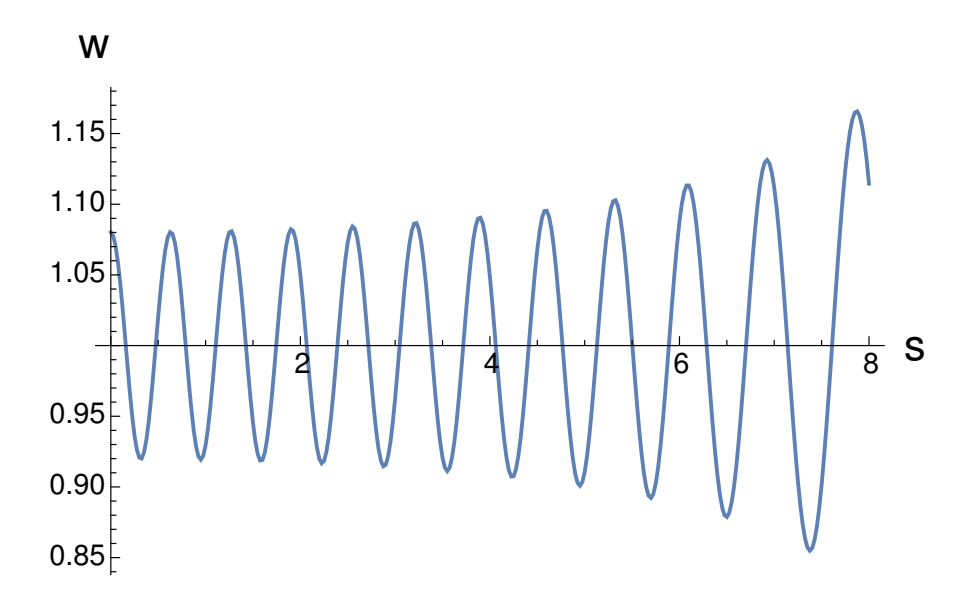


FIG. 6. Oscillation of the integral $w_{50}(s)$, defined by Eq. (5) with N=50.

Furthermore, the "cut weight", defined as

$$w_N(s) = \int_{-\infty}^{\infty} dr D_N(r, s), \qquad (5)$$

ideally should be close to 1. Yet, as illustrated in Fig. 6, it strongly oscillates as a function of the cut position s. For N=50 the oscillation varies between ≈ 0.92 and ≈ 1.08 . This amplitude decreases very slowly as N increases. For N=200, it still lies between ≈ 0.96 and ≈ 1.04 , as shown in Fig. 7.

The strong increase in oscillation frequency clearly comes from the growing degrees of the polynomials shown by Eq. (A2).

Figure 8 shows, for N = 200, several cut shapes. The values of s are 0, 2, 5, 9, 14 and 19, respectively. There is clear evolution of the shapes between s = 0 and s = 19, but the peaks are observed to follow the decrease of the ridge crest. By comparison, the cut weight, $w_{200}(s)$, displayed in Fig. 7 oscillates around the optimal value 1.

We also produced intermediate results as a check, corresponding to N = 100 and N = 150. Those results confirm the results displayed herein, that there is some convergence as N increases, and so are not shown in the following discussions. However, that convergence we had found to be slow.

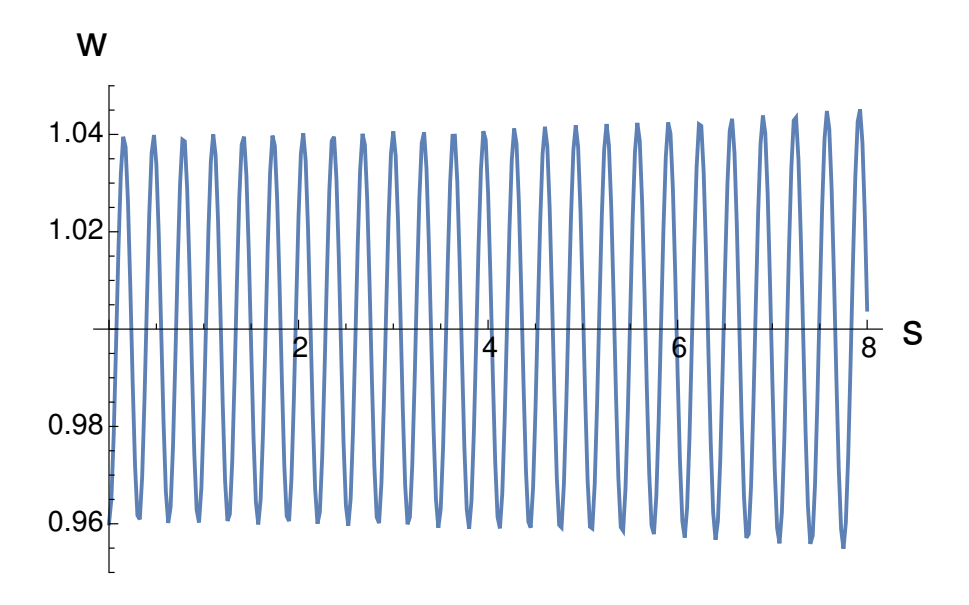


FIG. 7. As for Fig. 6, but for N = 200.

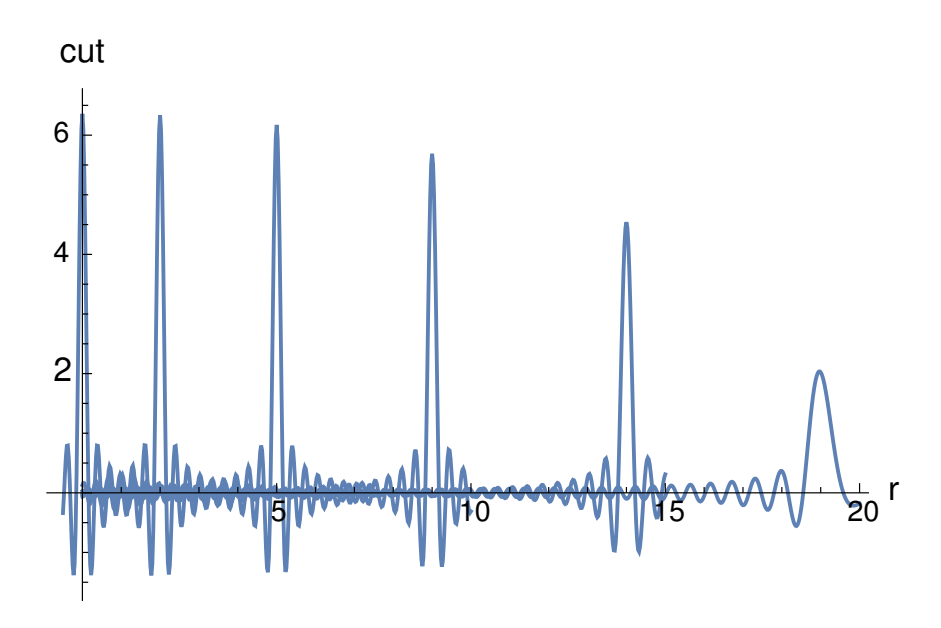


FIG. 8. Cut shapes for N=200. Positions s=0,2,5,9,14,19.

III. QUALITY OF THE RECONSTRUCTION OF THE KINETIC ENERGY OPERATOR

Turning our attention to the kinetic energy operator where locality features are expected if we work in the momentum space representation, we wish to observe how this operator, $-d^2/dr^2$, is reconstructed in the coordinate space representation. Hence, we consider kernels

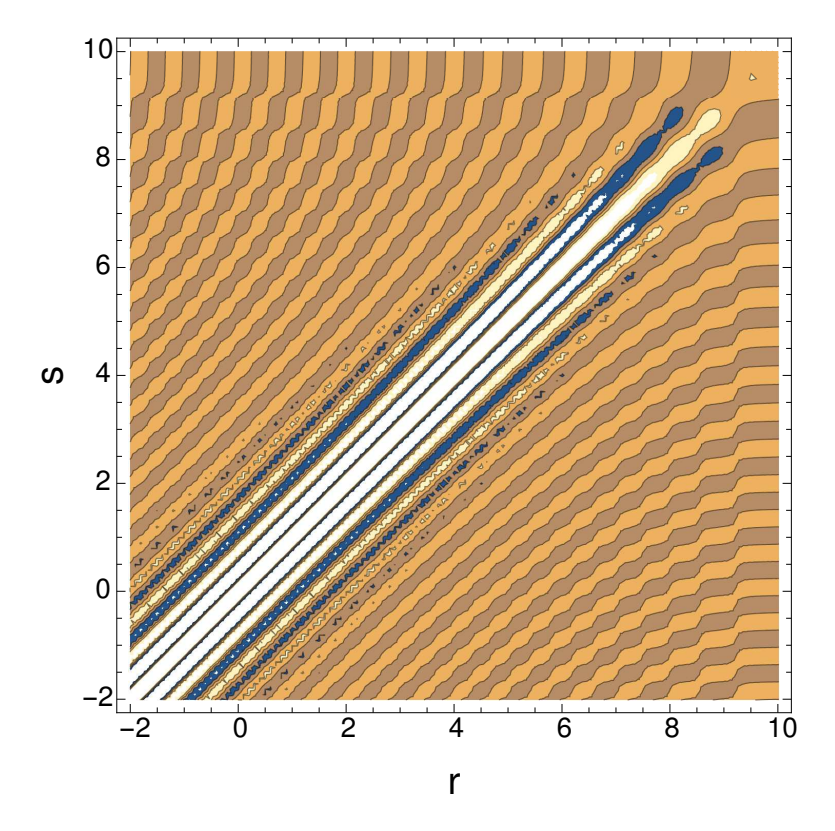


FIG. 9. Reconstruction of the kinetic operator; contour plot when N=50.

of the form,

$$\Theta_{N}(r,s) = \sum_{i,j=1}^{N} \varphi_{i}(r) \left\langle i \left| \left(-\frac{d^{2}}{dr^{2}} \right) \right| j \right\rangle \varphi_{j}(s).$$
 (6)

Again, symmetries under the transformations $\{r, s\} \to \{s, r\}$ and $\{r, s\} \to \{-r, -s\}$ are trivial.

Figure 9, obtained with N=50, shows a pattern along the diagonal r=s. When a cut is implemented by freezing s, it exhibits a positive peak which is flanked by two negative peaks of roughly half its surface, effectively emulating a $-\delta''$ function. However, further oscillations do not improve matters, as shown in Fig. 10, with s=0 and s=6 for N=50. A distortion of the shape of the cut is observed at s=6, and is explained by its position near the end of the range of validity which is limited by 50 components in the basis. The crest ridge, as also displayed in Fig. 10, exhibits a shape which touches the tops of the cuts tangentially, as expected.

Ideally, the approximation of the second derivative of the δ function, $\Theta_{N}(r,s)$, should

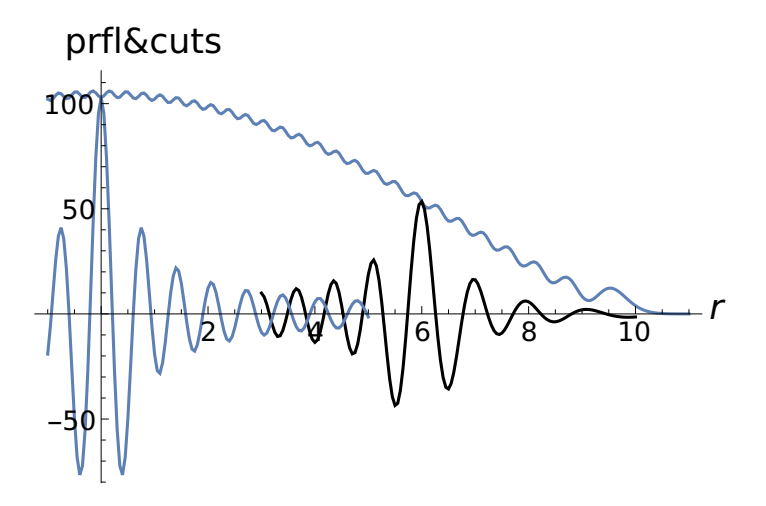


FIG. 10. The "kinetic reconstruction" for N=50. The crest and cut shapes, $\Theta(r,r)$, $\Theta(r,0)$, $\Theta(r,6)$, are displayed.

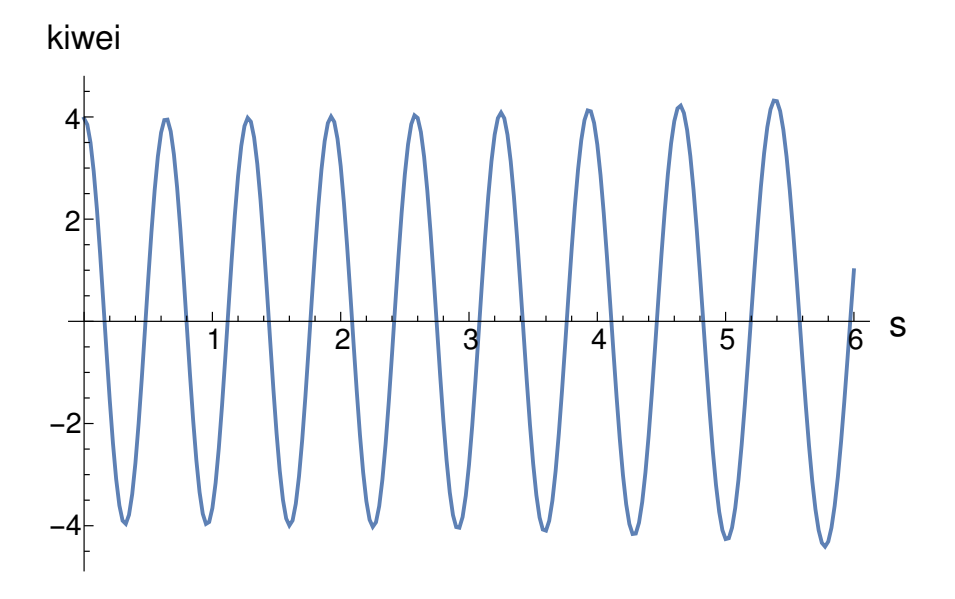


FIG. 11. The weight, given by Eq. (7), from the "kinetic reconstruction" of the second derivative of the δ function for N=50.

have a vanishing weight, given $\forall s$ by,

$$w_{ki} = \int_{-\infty}^{\infty} dr \,\Theta_N(r, s) \,. \tag{7}$$

However, as shown in Fig. 11, for N=50, the weight oscillates strongly as a function of s, with amplitude ≈ 4 . That amplitude grows to ≈ 8 for N=200. This does not indicate an encouragingly fast convergence towards the exact δ'' function. The observed high oscillation

frequency in the "noise" of Θ_N has the same origin as that in the "noise" of D_N , namely the occurrence of high degree polynomials in its compact formula. See the Appendix for the corresponding Christoffel-Darboux-like extension to that case, very similar to Eq. (A5).

In order to understand any convergence, we consider a different approach and diagonalise the matrix built by the matrix elements

$$\left\langle i \left| \left(-\frac{d^2}{dr^2} \right) \right| j \right\rangle, \quad i, j = 1, \dots, N.$$
 (8)

From the matrix, we obtain the lowest eigenvector components c_i , i = 1, ..., N, square normalised to unity, and consider the corresponding wave function

$$\psi_{1,N}(r) = \sum_{i=1}^{N} c_i \varphi_i(r). \tag{9}$$

The spectrum of the true kinetic energy operator is continuous with a lower bound of 0. Hence, in the present matrix approximation, the wave function, $\psi_{1,N}(r)$, should be as smooth and flat as possible to simulate a wave without momentum. Indeed, the waves $\psi_{1,50}$ and $\psi_{1,200}$ are positive parity and reasonably flat. The former extends between $\approx \pm 10$ until it exponentially decays. It reaches a maximum of 0.32. For the latter, the range and maximum values read $\approx \pm 20$ and ≈ 0.22 , respectively. Hence, at the cost of multiplying the number of components by 4, one obtains ratios of ≈ 2 for the ranges, which seems reasonable, and $\approx 0.22/0.43 = 0.69$ for the flatness. A rule of thumb for square normalisation as the range doubles would predict a scaling of $1/\sqrt{2} \approx 0.71$ for the wave function, which is close to the observed ratio. These latter considerations may attenuate the possible doubts suggested by the oscillations seen above.

IV. RECONSTRUCTION OF POTENTIALS

A. Simple, local potentials

A local potential, v, by definition, is given by the matrix element between states $|r\rangle$ and $|s\rangle$, viz.

$$\langle r | v | s \rangle = v(r) \delta(r - s)$$

= $v\left(\frac{r+s}{2}\right) \delta(r-s)$, (10)

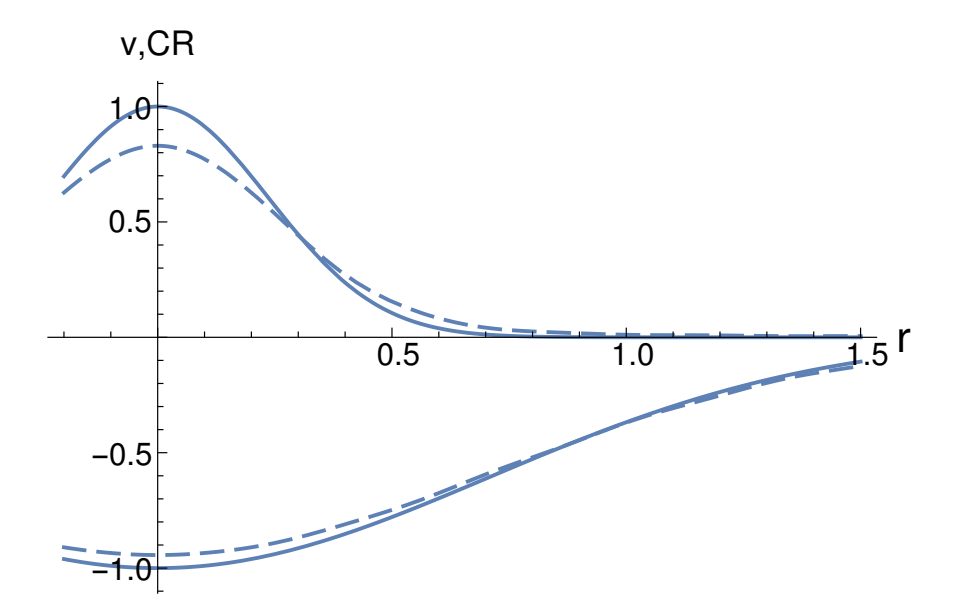


FIG. 12. The potentials v (solid lines) along the crest of their finite matrix kernels \mathcal{V} for N=50. The crest ratios [Eq. (12)] are portrayed by the dashed lines. (See also the discussion in text.)

where the second equation is of a more symmetric form. With this definition of the local potential, we may form the kernels

$$\mathcal{V}_{N}(r,s) = \sum_{i,j=1}^{N} \varphi_{i}(r) \langle i | v | j \rangle \varphi_{j}(s)$$
(11)

and assess if the kernel forms a reasonable representation of the local potential. Further, we may investigate whether the intuitive ansatz, $D_N(r,s)v\left(\frac{r+s}{2}\right)$ itself makes a reasonable approximation of \mathcal{V}_N if D_N is a suitable approximation of the δ function as discussed in Section II.

We first consider the local potentials $v(r) = -e^{-r^2}$ and $v(r) = e^{-9r^2}$. The (one-dimensional) harmonic oscillator basis used herein has as its "germ" the basic Gaussian $\pi^{-1/4}\beta^{-1/2}e^{-r^2/(2\beta^2)}$, with the length scale $\beta = 1$. The two potentials then can be considered as a moderate-range attractive potential and a short-range repulsive potential, respectively. The crest ratio (hereafter CR), defined as

$$CR = \frac{\mathcal{V}_N(r,r)}{D_N(r,r)},\tag{12}$$

is displayed in Fig. 12, for N = 50.

Therein, the crest ratios are portrayed by the dashed lines while the potentials themselves are portrayed by the solid lines. The approximation of the moderate-range potential shows

an error of at most $\approx 6\%$ when comparing the potential to its CR while the error in the approximation for the short-range potential worsens to $\approx 17\%$. When one increases N to a value of 200, the errors reduce to 3% and 8%, respectively, with the reduction in the error of a factor of 2, indicating a reasonable convergence to the actual potentials.

B. The case of r^2

The reconstruction of the kinetic energy operator was somewhat problematic. Similar problems may be expected for the case of reconstruction of r^2 since, except for pure phases under a Fourier transformation, harmonic oscillator wave functions are the same in both the coordinate and momentum space representations. The reconstruction of the r^2 operator in coordinate space is a perfect image of the reconstruction of its kinetic partner, p^2 , in momentum space. We define

$$\mathcal{R}_{N}(r,s) = \sum_{i,j=1}^{N} \varphi_{i}(r) \left\langle i \left| r^{2} \right| j \right\rangle \varphi_{j}(s).$$
(13)

A compact form of this sum is available in the Appendix, see Eq. (A5). Figure 13 shows the contour plot of $\mathcal{R}_{50}(r,s)$. There is a notable ridge pattern along the diagonal axis, r=s. If one compares the results in Fig. 13 with those of Fig. 1, one finds more oscillations in the contour plot in Fig. 13, a low region around the origin, r=s=0, and then a rise in the ridge until an exponential collapse when either |r| or $|s| \approx 11$. Recall, that in Section II for the case of N=50, the range beyond which the basis could not be trusted was ≈ 7 . See again the Appendix for the rich pattern of oscillations.

At the origin, r = s = 0, the CR is worth $\frac{1}{2}$ and does not depend on N. The ratios, $\mathcal{R}_N(1,1)/D_N(1,1)$, $\mathcal{R}_N(2,2)/D_N(2,2)$, and $\mathcal{R}_N(3,3)/D_N(3,3)$, are shown in Fig. 14 as functions of N. They fluctuate around 1.5, 4.5 and 9.5, respectively. More generally, the ratio $\mathcal{R}_N(r,r)/D_N(r,r)$ converges slowly towards $r^2 + 1/2$ as N increases.

By evaluating the eigenstates of the matrix

$$\rho_N = \{ \langle i | r^2 | j \rangle, i, j = 1, \dots, N \},$$
(14)

these observations of an insufficient quality of the matrix reconstruction of r^2 may be completed. We let N be the number of basis components and c_j the components, square normalised to unity, of any of the eigenvectors of ρ_N , with λ the corresponding eigenvalue.

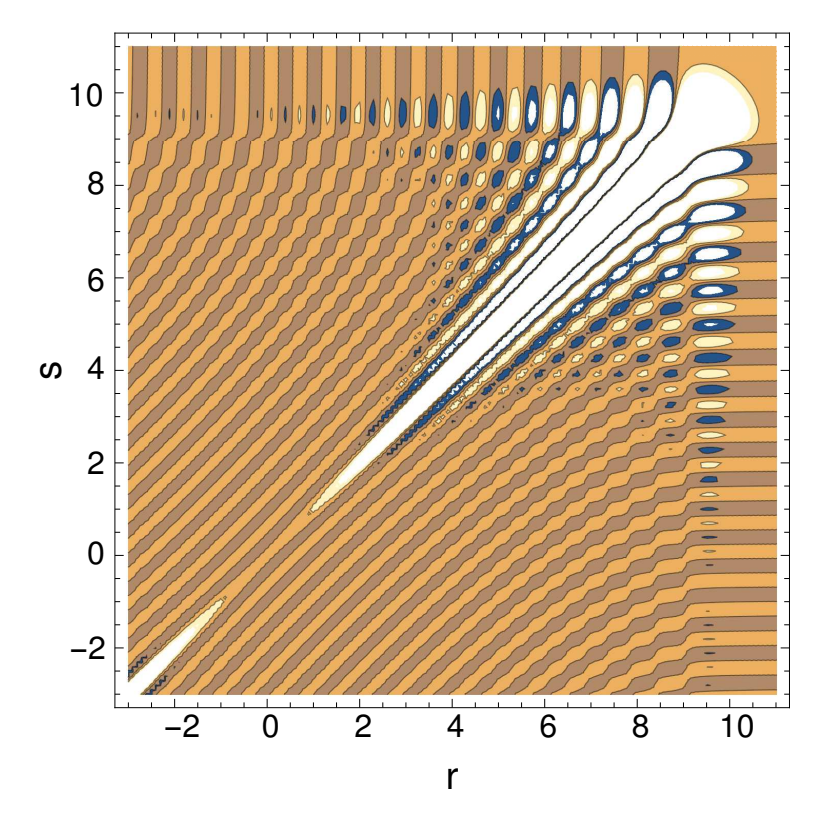


FIG. 13. The contour plot of $\mathcal{R}_{50}(r,s)$, the reconstruction of the r^2 operator.

Hence

$$\sum_{j} \rho_{kj} c_j = \lambda c_k. \tag{15}$$

If we consider the wave function,

$$\psi(r) = \sum_{j} c_{j} \varphi_{j}(r) \tag{16}$$

we find that ψ is an eigenstate of the kernel \mathcal{R} given that

$$\int_{-\infty}^{\infty} \mathcal{R}(r,s) \,\psi(s) \, ds = \lambda \psi(r) \,. \tag{17}$$

And, given that \mathcal{R} may be considered an acceptable approximation of r^2 , then ψ may be considered a reasonable approximation of an eigenstate of the operator r^2 .

For the following, we return to the original definitions of the variables: the index i is again associated with the eigenstate of ρ_N , represented by the $\{c_j\}$ and where N is the component number. As r^2 is a local operator whose eigenstates are represented by δ functions, we expect that the $\psi_{i,N}$ become narrower as N increases. That is the case as shown in Fig. 15.

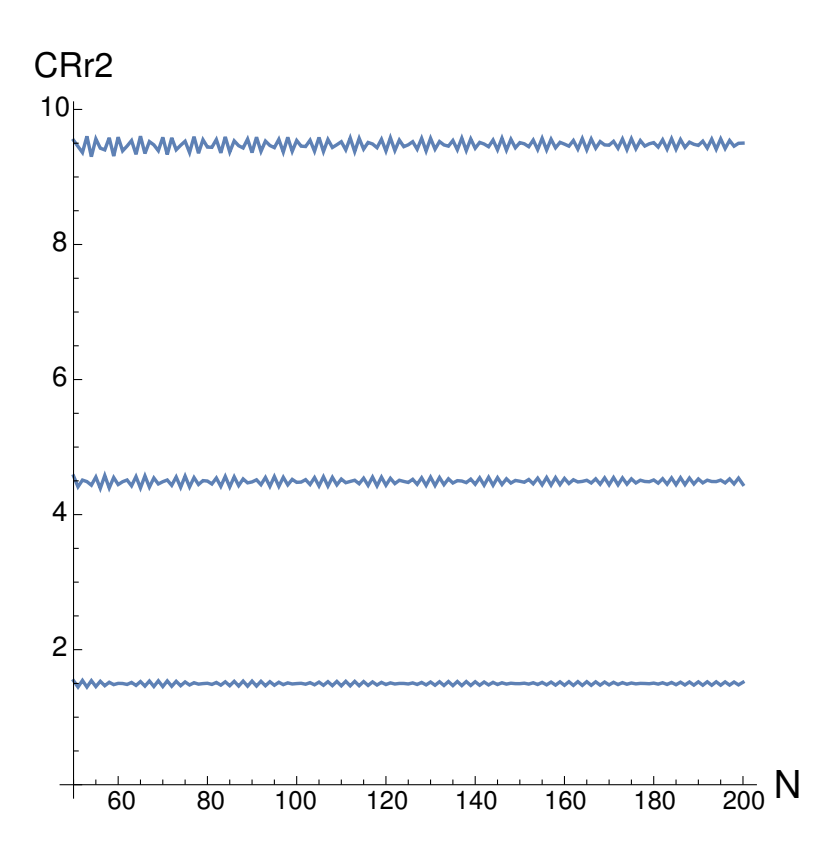


FIG. 14. The reconstruction of r^2 . The horizontal lines are crest ratios as functions of N. r = 1, 2, 3, the CR fluctuates about 1.5, 4.5, 9.5, respectively.

Note that a slight, somewhat irrelevant, complication is brought by parity, a property of the matrix ρ_N . Except for the ground states $\psi_{1,N}$, which are centered at the origin, the good parity states $\psi_{i,N}$, $i=2,\ldots,N$ are made of pairs of peaks. For graphical convenience, Fig. 15, shows only those peaks that are on the positive side of the r axis.

The eigenvalues for the ground states, in the cases of N=50 and N=200, are $\lambda_{1,50}=0.0244$ and $\lambda_{1,200}=0.0062$. The width of the wave packet $\psi_{1,200}$ is close to half that of $\psi_{1,50}$, and its height is multiplied by $\approx \sqrt{2}$. This is expected and an indication of convergence as N increases. Along with the ground states, Fig. 15 shows $\psi_{30,50}$, $\psi_{50,50}$, $\psi_{30,200}$, $\psi_{50,200}$, and $\psi_{120,200}$. For graphical convenience, and for comparison purposes, the peaks for N=200 are shown as mainly positive functions while those peaks for N=50 are negative functions. It is evident that the peaks decrease in width and increase in height as N increases. This confirms the convergence, albeit a slow one.

One may also consider whether the sum $\Theta + \mathcal{R}$ [(Eqs. (6) and (13)], which in these cases gives exact eigenvalues, $\Lambda_i = (2i - 1)$, while separately with each generated term giving

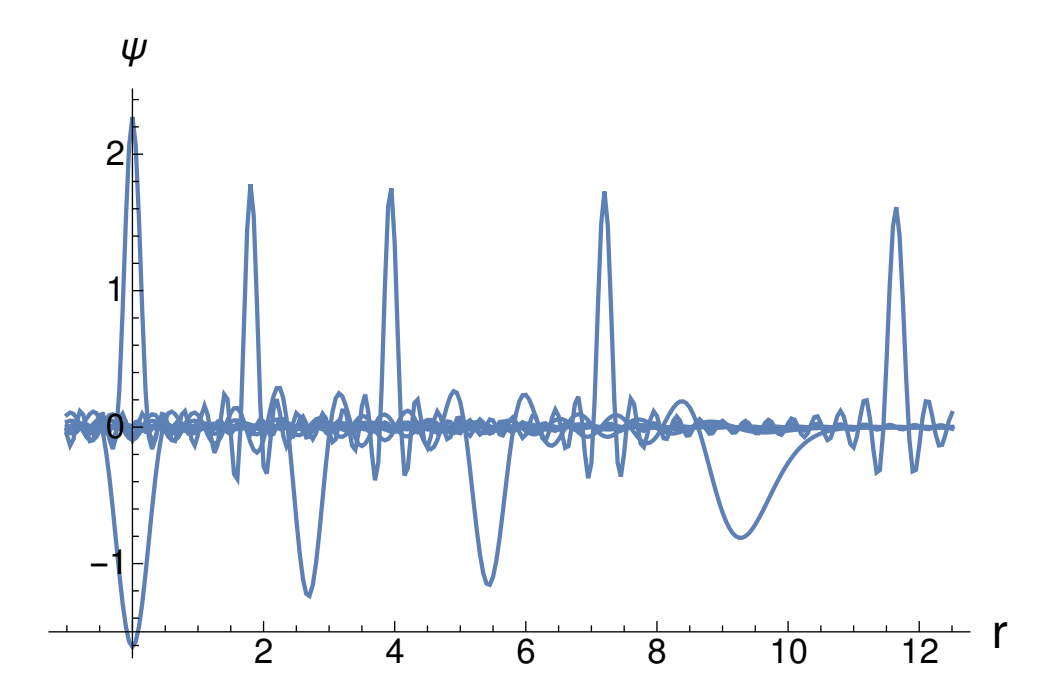


FIG. 15. The following localised states, as obtained by diagonalising finite matrix approximations of r^2 , are displayed. Peaks above the **r**-axis: $\psi_{1,200}$, $\psi_{30,200}$, $\psi_{50,200}$, and $\psi_{120,200}$. Below the axis: $\psi_{1,50}$, $\psi_{30,50}$, and $\psi_{50,50}$. (See the text for details.)

somewhat imprecise results, would still yield reasonable results if the choice of the functions $\{\varphi_i\}$ were different. Difficulties with Eqs. (6) and (13) are almost guaranteed, as these attempt to reproduce operators that have continuous spectra by operators of finite rank. But, with a different basis, the sum $\Theta + \mathcal{R}$, being still an approximation of $-d/dr^2 + r^2$, and likely having a discrete spectrum, may still permit good approximations of eigenvalues, given that errors at first order in wave functions translate to second order for the eigenvalues. See Section V for a numerical illustration.

C. Separable potentials

Let $|\xi\rangle$ denote the form factor, assumed to be real, so that the potential becomes separable: $\xi(r)\xi(s)$. Eq. (11) may then be written as

$$W_{N}(r,s) = \left[\sum_{i=1}^{N} \varphi_{i}(r) \langle i|\xi\rangle\right] \left[\sum_{j=1}^{N} \langle \xi|j\rangle \varphi_{j}(s)\right]. \tag{18}$$

The quality of the separable representation is governed by the quality of the form factor, $|\xi_N\rangle = \sum_{i=1}^N \langle i|\xi\rangle |i\rangle$. The question of convergence reduces to that of convergence in the

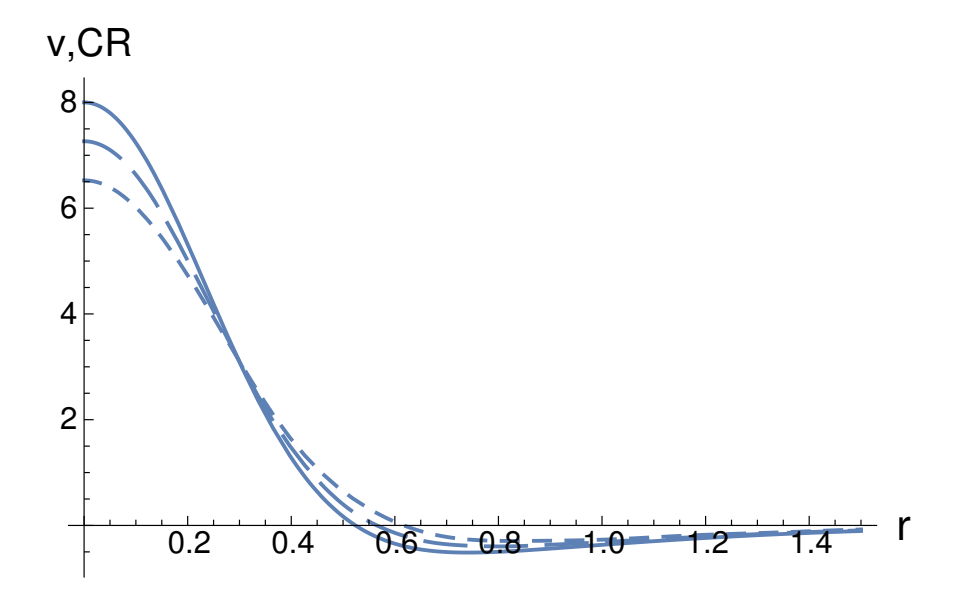


FIG. 16. The reconstructed semi-realistic potential using the CR method. See text for details. context of square integrability.

D. Semi-realistic potential

We use the potential

$$v(r) = 9e^{-9r^2} - e^{-r^2}, (19)$$

which combines a strong repulsive core and a mid-range attraction. Figure 16 shows the potential as a full line, its somewhat acceptable reconstruction by the "CR method" with N=200 as a long dash curve, and the weaker result for N=50 as a smaller dash curve. Overall, the results of the approximations using the CR method are acceptable, except near r=0.

E. Extension to a toy Hamiltonian

In this case we continue the investigation by generalising to a toy Hamiltonian

$$h = -\frac{d^2}{dr^2} + e^{-9r^2} - e^{-r^2} \tag{20}$$

where we have mixed the repulsive core and the attractive term in proportions that allow for a bound state, simplifying the numerics. The exact ground state, $\psi_{\rm ex}$, has the eigenvalue $\varepsilon_{\rm ex} = -0.1720763$. We then project h onto subspaces with bases of, for example, 50 and 100 of the oscillator wave functions. (The subspaces may be further reduced to bases of 25 and 50 states due to parity conservation.) The ground state eigenvalues found in those subspaces are $\varepsilon_{50} = -0.171874$ and $\varepsilon_{100} = -0.172071$, respectively. This is a reasonable result and the comparison of the respective ground states shows quite small errors of the order of 10^{-2} and 10^{-4} for N = 50 and N = 100, respectively.

V. DIFFERENT SINGLE PARTICLE BASIS

The simplicity and convenience of the harmonic oscillator basis does not always guarantee fast enough convergence. We now consider an alternative set of basis functions, namely an even number N of translated Gaussians,

$$\varphi_i(r) = \pi^{-\frac{1}{4}} \beta^{-\frac{1}{2}} \exp\left[-\frac{\left(r + \frac{N+1}{2}\sigma - i\sigma\right)^2}{2\beta^2}\right], i = 1, \dots, N.$$
(21)

Therein, σ is a shift parameter. The basis formed by these functions exhibits, except for edge effects, an approximate translational invariance. However, the basis needs to be orthonormalised into a set of functions $\{\chi_i(r), i=1,\ldots,N\}$. The orthonormalisation process is not unique and we tested two processes; the results do not depend on the process, as expected.

When σ is significantly smaller than the width of the Gaussians, taken again with $\beta = 1$, the orthogonalisation process involves derivatives and can reconstruct something similar to the harmonic oscillator basis. For that reason, we take $\sigma = \beta$ instead. This choice separates each Gaussian from its neighbours, somewhat moderately, leading to finite difference effects rather than approximate derivatives. It also defines an efficiency range, of the order of $N\sigma/2$ at the minimum. Upon inspection, one of our new bases may still show states with some similarity to the oscillator states but the corresponding width parameter, β_{new} , would be significantly larger than β .

When N=50, the first seven lowest eigenvalues of the matrix approximation of $-d^2/dr^2+r^2$ with this new basis are, $\{1.00043, 3.00005, 5.05263, 7.0184, 9.6656, 11.3889, 15.7908...\}$, to be compared with the exact sequence $\{1, 3, 5, 7, 9, 11, 13...\}$. While the approximation is seen to be quite good at first, an onset of worsening accuracy occurs after the 5th or 6th eigenvalue. This is to be expected.

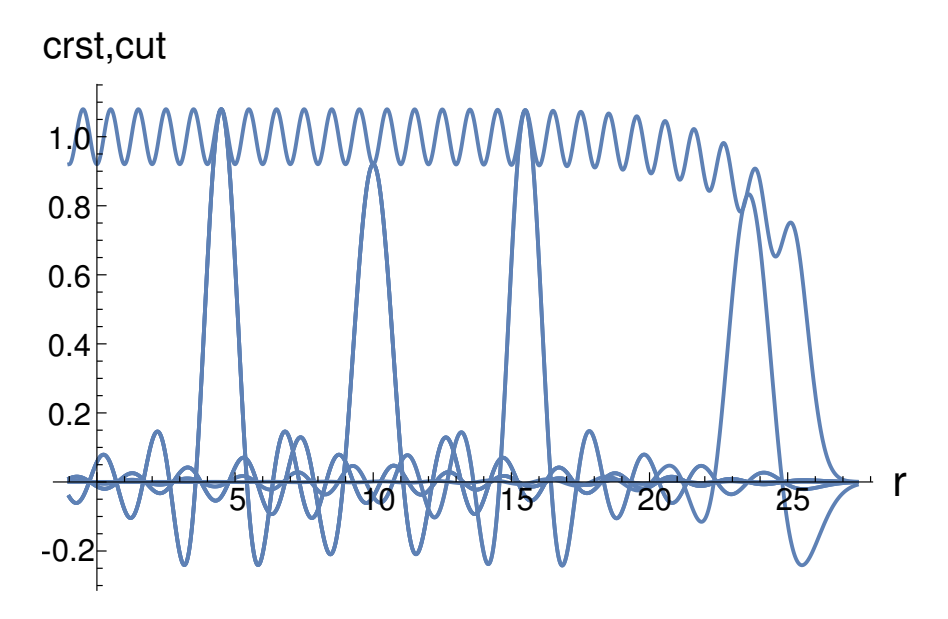


FIG. 17. The profile of the crest, and of the cuts at s = 4.5, 10, 15.5, 23.5, using the new basis with $\beta = \sigma = 1, N = 50$.

We return to the approximation of the δ function which, in terms of the normalised new basis states, is written as $\Delta_N(r,s) = \sum_{i=1}^N \chi_i(r) \chi_i(s)$. And, to confirm our numerical results, we also generated the same, self-replicating, kernel as $\Delta_N(r,s) = \sum_{i=1}^N \varphi_i(r) \tau_i(s)$, introducing the dual space spanned by the basis states τ_i with $\langle \tau_i | \varphi_j \rangle = \delta_{ij}$; that basis can be obtained by inverting the matrix of scalar products $\langle \varphi_i | \varphi_j \rangle$. For N = 50 and the new basis of shifted Gaussians, the contour plot of Δ_{50} resembles that displayed in Fig. 1 for D_{50} . Yet significant differences exist.

As shown in Fig. 17 the crest now shows an almost horizontal trend except for residual oscillations. Also, with an "efficiency range" of ≈ 12 , the cuts seems to be similar to one another, suggesting a reasonable stability in the approximation. Further, as long as |s| is less than ≈ 12 , the "weight", defined by

$$w = \int_{-\infty}^{\infty} \Delta(r, s) dr, \qquad (22)$$

remains close to 1, as illustrated in Fig. 18.

As a final study with an alternative basis, we now reconstruct the semi-realistic potential given by Eq. (19). However, as the potential has an exponential decay beyond $r \approx 2$, it is not very useful to consider shifted Gaussians beyond this value of r. We choose instead a

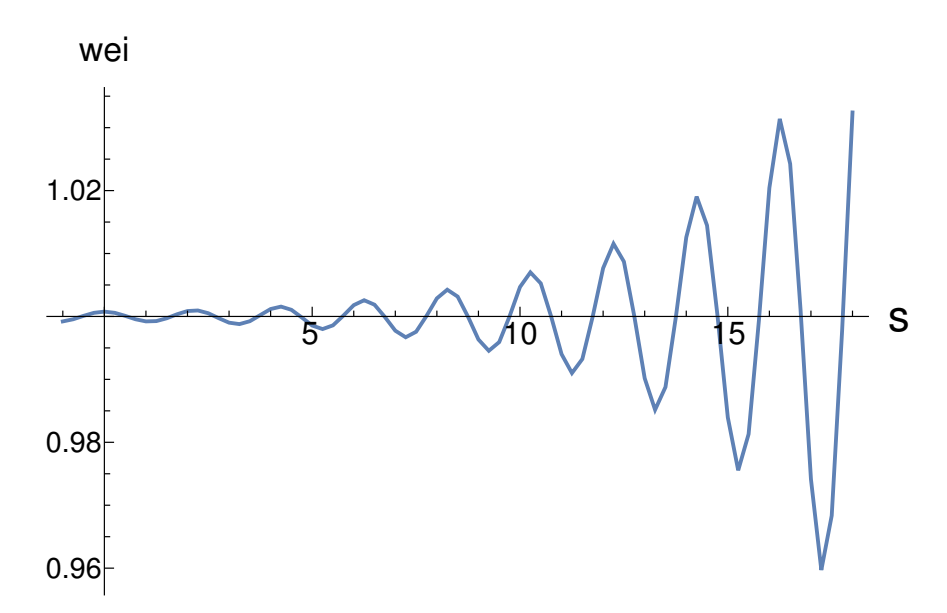


FIG. 18. The weight function, Eq. (22), obtained using the same basis as that in Fig. 17.

basis set,

$$\varphi_i(r) = \pi^{\frac{1}{4}} \beta^{-\frac{1}{2}} \exp\left[-\frac{(r - r_c)^2}{2\beta^2}\right],$$
(23)

where $r_c = i\sigma - (N + 1/2) \sigma$, i = 1, ..., N. We take $\beta = \sigma = 0.1$, for an example, and set N = 40 and N = 60 as two comparison reconstructions. The former value of N provides an effective range of ≈ 2 and the latter value a range of ≈ 3 . Figure 19 shows the results of the reconstructions, where v_{40} and v_{60} are the potentials found for N = 40 and 60, respectively, both using the CR method. In that figure, the actual results for both values of N are practically equal, and so only v_{60} is portrayed. Indeed, both give very reasonable reproductions of the original potential. To highlight the difference between the two results, we also give the difference $v_{60} - v_{40}$ multiplied by 1000.

VI. SINGLE PARTICLE BASIS TAKING ADVANTAGE OF SYMMETRY

We consider again the toy Hamiltonian of Eq. (20). We wish to compare its exact ground state, $\psi_{\rm ex}$, with eigenvalue $\varepsilon_{\rm ex} = -0.172076$, with the approximate ground state ψ_N and its eigenvalue when the Hamiltonian is projected onto one of the subspaces. The ground state

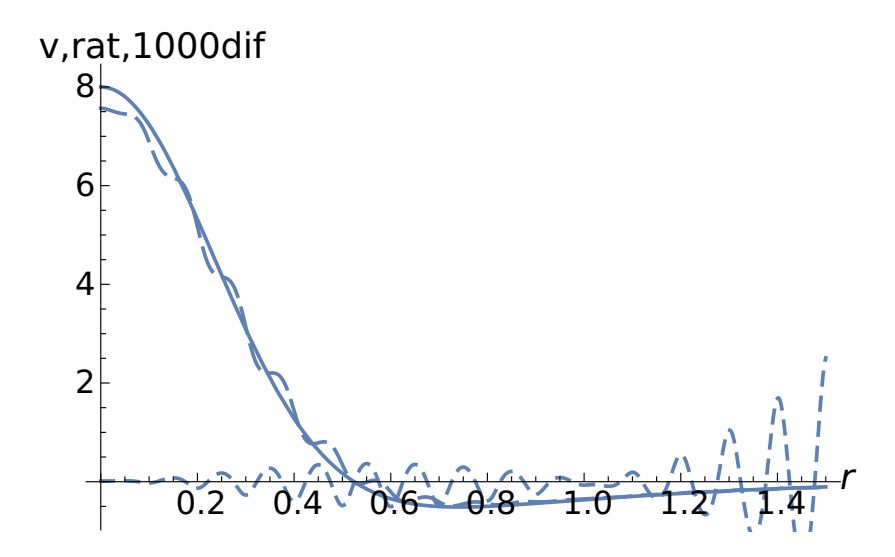


FIG. 19. The potential. The solid line portrays the full function. The long-dashed line is that which is approximated using a basis of 60 shifted Gaussians, using the CR method. The short-dashed line is the expanded difference between the potential created using 60 basis states and that created using 40 basis states, viz., $1000 (v_{60} - v_{40})$.

is even under parity and so we consider a "raw" basis of pairs of basis states

$$\varphi_i(r) = \frac{1}{\sqrt{2}} \pi^{\frac{1}{4}} \beta^{-\frac{1}{2}} \left[e^{-(r-r_c)^2/(2\beta^2)} + e^{-(r+r_c)^2/(2\beta^2)} \right], \tag{24}$$

where $r_c = (i - \frac{1}{2}) \sigma$, i = 1, ..., N, and with the understanding that this basis is constructed before orthonormalisation.

Figure 20 shows the contour plot of the idempotent kernel, $\Delta_N(r,s) = \sum_{i=1}^N \chi_i(r) \chi_i(s)$, for N=25 and $\beta=\sigma=1/2$. This choice spreads the basis states, and their orthonormalised forms χ_i , in a range $|r| \lesssim 12$. Note, that for the line r=-s, there is an additional ridge due to parity. Small interference effects are noticeable near r=s=0, which are due to those few wave packets of the raw basis that are close to the origin. The pair of ridges provide an approximation of the sum $[\delta(r-s)+\delta(r+s)]/2$, from which there has to be a positive interference near the origin. That is observed in Fig. 20 when $r,s\lesssim 1$. The crest profile shows a flat trend, perturbed by the expected oscillations, between $r=s\approx 1$, and $r=s\approx 10$. This suggests the stability of the approximation in those domains.

For N=25, the approximate ground state of the toy Hamiltonian has an eigenvalue $\varepsilon_{25}=-0.17194$. compared to the exact value of $\varepsilon_{\rm ex}=-0.17208$. The eigenvalue for N=25 is a reasonable result, better than the value obtained using harmonic oscillator states at

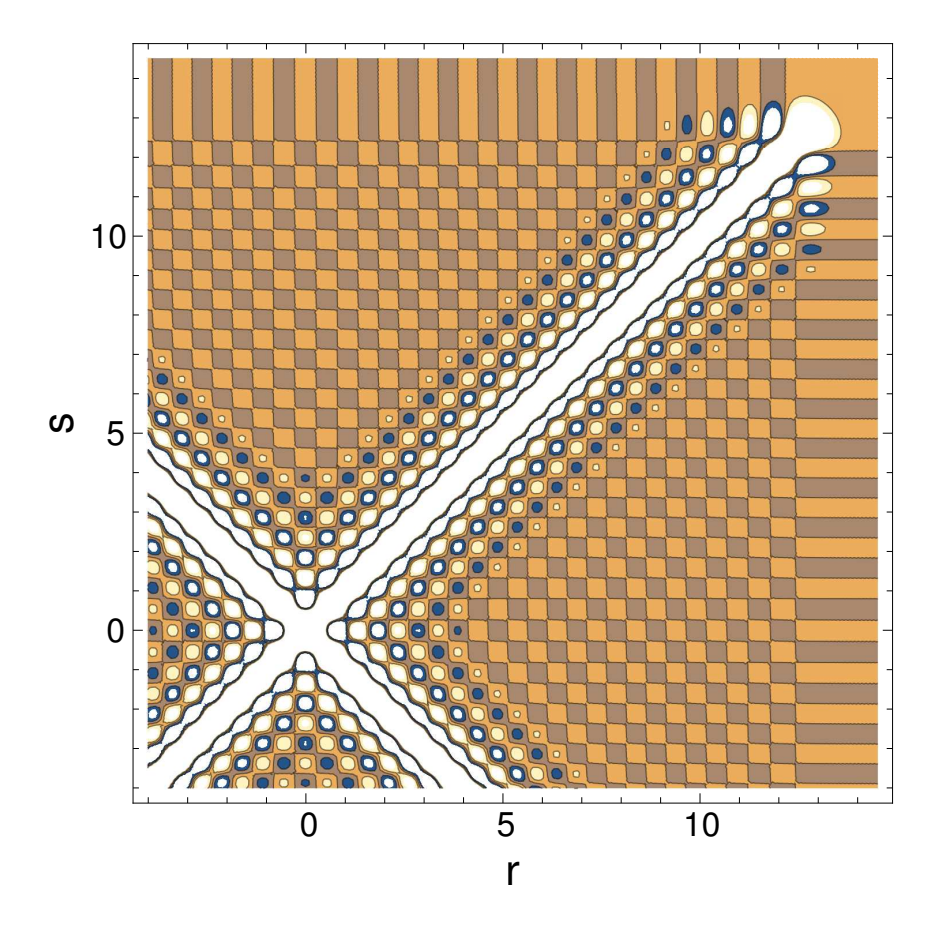


FIG. 20. The contour plot of Δ found using a basis of 25 pairs of symmetrically shifted Gaussians with $\beta = \sigma = \frac{1}{2}$.

 $N=50,\ \varepsilon_{50}=-0.17187.$ The "weight", $w\left(s\right)=\int_{-\infty}^{\infty}\Delta\left(r,s\right)\,dr$ remains close to 1, with limited oscillations, in the range $0.96\lesssim w\left(s\right)<1.04.$ The observed range of $w\left(s\right)$ is within a somewhat large domain $|s|\lesssim 8$, as shown in Fig. 21, despite its fragmentation between the simulations of $\frac{1}{2}\delta\left(r-s\right)$ and $\frac{1}{2}\delta\left(r+s\right)$. Finally, the difference between the approximate wave function and the exact one for this toy Hamiltonian, $\psi_{25}-\psi_{\rm ex}$, is of order $\approx 10^{-2}$ at most.

In the case of N=50, an accuracy of one more decimal place is required given the way ε_{50} converges to the exact eigenvalue, and also in the way ψ_{50} converges to the exact wave function. Two more decimal places are found to see any variation in w(s) near unity. Those good results are partly misleading, however, given that we took the precaution of verifying the reconstructions of the kinetic and potential energy operators in earlier sections. For such operators individually no truly satisfactory result was obtained; looking at the Hamiltonian in full produced a far better convergence.

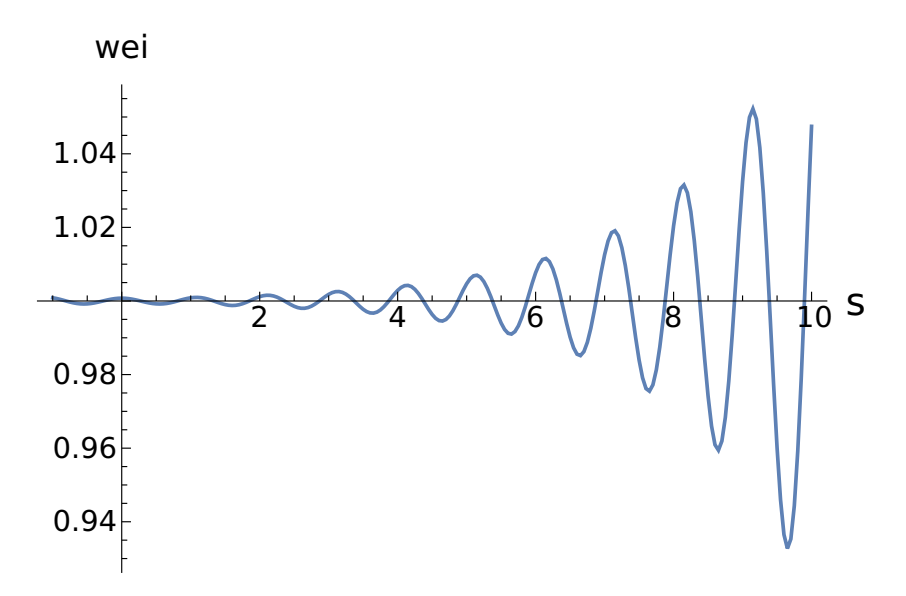


FIG. 21. The basis from 25 pairs of Gaussians. Also displayed is the evolution of the weight w(s) of a cut at given s.

VII. EFFECTIVE FORCES

We now consider the Feshbach projection formalism, namely to split the full Hilbert space into two or three subspaces. (See refs [9, 10].) Following the approach of Karataglidis and Amos [1] (hereafter KA), the subspaces are created by the use of projectors $\mathcal{P} = \sum_{i=1}^{N_1} |\chi_i\rangle \langle \chi_i|$, $Q = \sum_{i=N_1+1}^{N_2} |\chi_i\rangle \langle \chi_i|$ and $\mathcal{R} = 1 - \mathcal{P} - \mathcal{Q}$. The subspaces are formed by projecting out the solutions to the Hamiltonian using these projectors. However, it may come to pass that the subspaces P and Q are not enough to span the entire Hilbert space and so the third subspace is required. The splitting of the Hilbert space into subspaces is necessary when truncation is required in the Hamiltonian matrix to allow for diagonalisation: the P subspace (the "included" space) is formed by the states which are found through direct diagonalisation of the truncated Hamiltonian, while the Q subspace (the "excluded" space) are those states that are not found through the diagonalisation. The effective Hamiltonian, which is reconstructed by use of the projection operators and the kernel, contains coupling between the P and Q subspaces, and R if necessary, to converge to the exact solutions.

For a one-dimensional toy model, for which we choose the Hamiltonian

$$h = -\frac{d^2}{dr^2} + 10e^{-9r^2} - 5e^{-r^2},$$
 (25)

we use a basis of harmonic oscillator even-parity states, and choose $N_1 = 5$ and $N_2 = 26$.

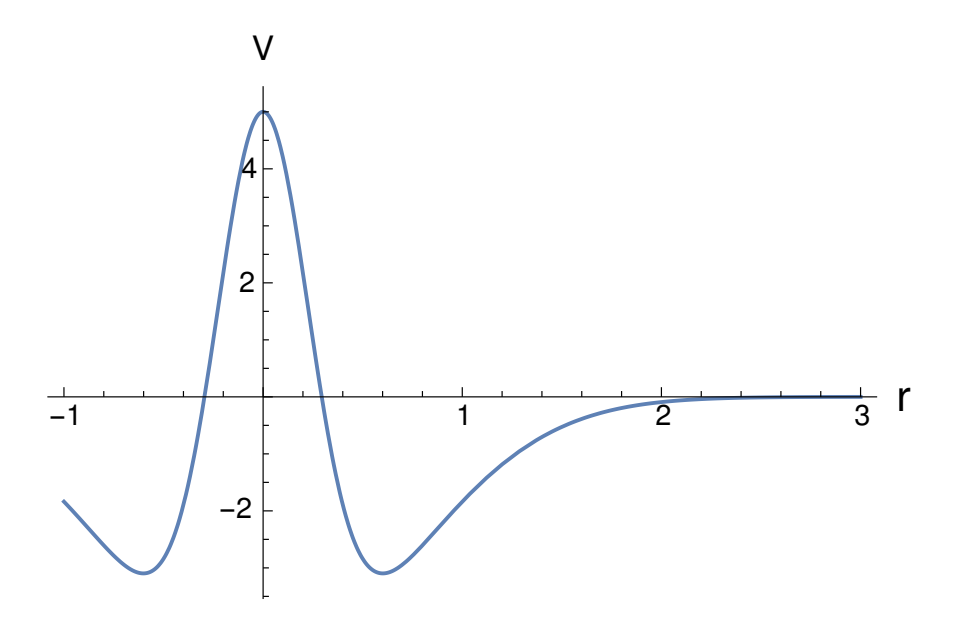


FIG. 22. Toy potential for a Feshbach method analysis.

This allows for a small P space with the Q space providing a significant correction to any results in the P space. The potential in Eq. (25) is shown in Fig. 22.

Consider first the P and Q subspaces only. The required matrices are PhP, PhQ, QhP, QhQ, with the kernel $G(E) = (E - QhQ)^{-1}$, from which we define the effective kernel $W_{\text{eff}} \equiv PhQG(E)QhP$. The diagonalisation of (P+Q)h(P+Q) yields a ground state energy $E_0 = -0.7342$ which compares favorably with the ground state eigenvalue, -0.7342256, obtained by numerical solution of the corresponding differential equation. (Notice, incidentally, that this availability of a precise numerical solution means that we have now activated the R subspace). The same diagonalisation of (P+Q)h(P+Q) also gives a very good approximation for the ground state wave function, ψ_0 . The comparison with the approximate reconstructions are shown in Fig. 23. Therein, the solid line is the best approximation. By construction, the diagonalisation of $PhP + W_{\text{eff}}$ gives the same energy eigenvalue $E_0 = -0.7342$ and the projected ground state wave function $P\psi_0$. The projected ground state, renormalised, is shown by the long-dashed line, and differs from that found by diagonalising only PhP, the result of which is portrayed by the short-dashed line. That wave function has a corresponding eigenvalue of $E_0^{\text{sub}} = -0.6897$, and which predictably under-binds.

The results obtained from such a toy model are sufficient to vindicate a use of matrix projections for *well-chosen* subspaces as tools for understanding and correcting eigenvalues

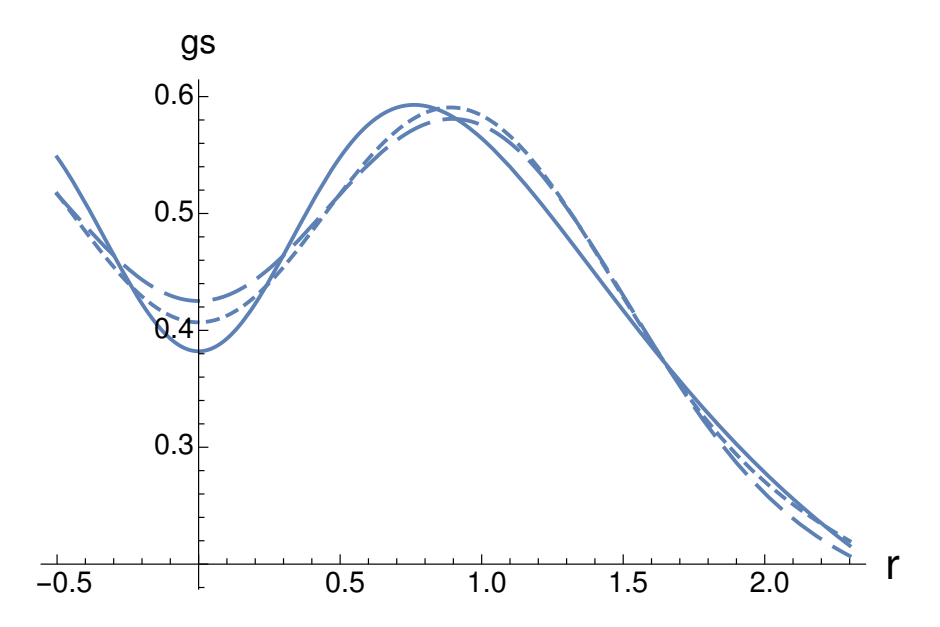


FIG. 23. Ground states for the Hamiltonian, Eq. (25). The results of the various calculations are given by: the solid line for $(\mathcal{P} + \mathcal{Q}) h (\mathcal{P} + \mathcal{Q})$; the long dash one for $\mathcal{P}h\mathcal{P} + W_{\text{eff}}(E_0)$; and the small dash one for $\mathcal{P}h\mathcal{P}$.

and eigenstates, although the previous sections show the limits of such projections. This cautious yet positive appraisal comes from the availability of powerful programs for numerical diagonalisations and inversions of matrices, even those with large dimensions.

A further note of caution. There is a convergence problem when \mathcal{P} and \mathcal{Q} are defined in such a way that, however large is their size, their is no way in which they might span the full Hilbert space. In that case, the R subspace, courtesy of its projector \mathcal{R} , restores the spanning of the Hilbert space. And if the R space is required, then convergence to the exact solution of both eigenvalues and states is difficult as the number of intermediate couplings in the effective Hamiltonian between the Q and R subspaces may be infinite [1].

This leads to the question of the effective potential: can W_{eff} be used to define a convenient, additional, energy-dependent, and (more or less) local potential for a diagonalisation in the P subspace? Formally, given the highlighted convergence problem, the answer would be negative. We show in Figs. 24 and 25 the contour plots for $\mathcal{P}h\mathcal{P}$ and W_{eff} , respectively. The contour plot for $\mathcal{P}h\mathcal{P}$ shows approximate ridge patterns, located around the lines $r = \pm s$, as expected for the quasi-locality of the toy Hamiltonian. However, the effective potential shown in Fig. 25 has no indication of any locality; the non-locality in W_{eff} is extreme.

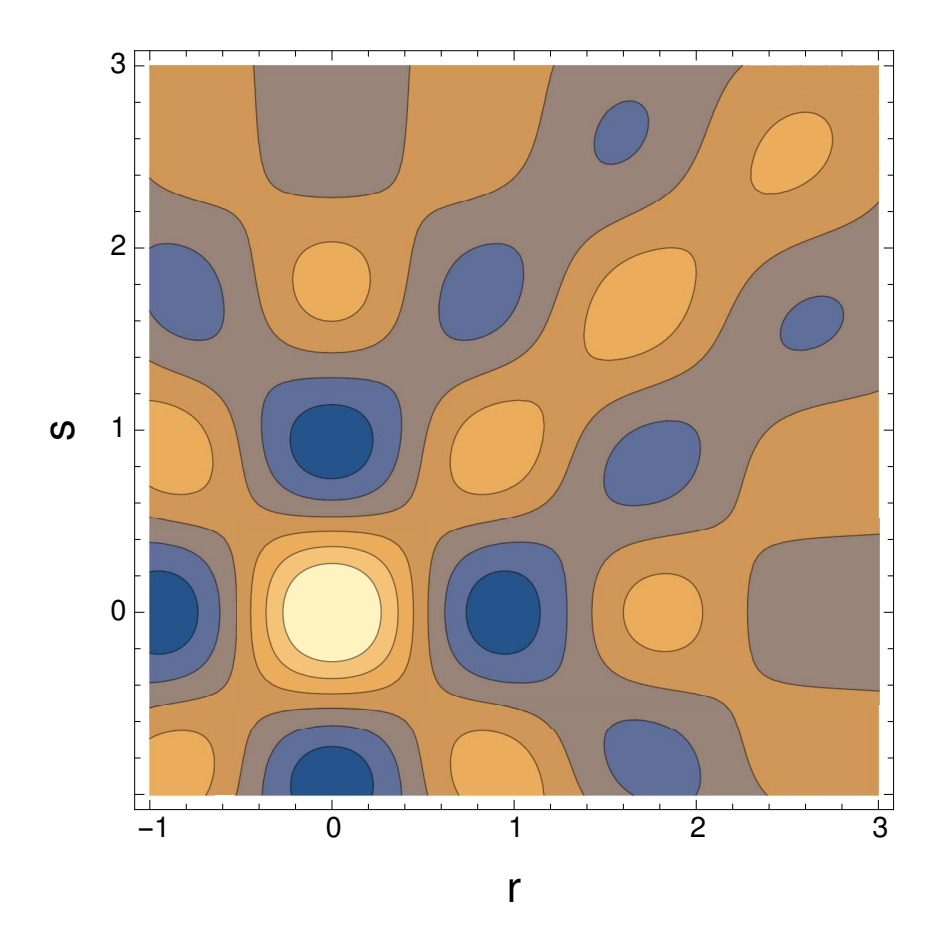


FIG. 24. N=5 contour plot for $\mathcal{P}h\mathcal{P}$. There is a vague hint of quasi locality along the diagonals $r=\pm s$.

VIII. SUMMARY AND CONCLUSIONS

Coined by Heisenberg, the term "matrix mechanics" extended the selection and description of atomic, molecular, and nuclear states from the bare quantum numbers of shells to a broader class of configuration mixings. The resulting calculations, ranging from valence mixings to large shell-model configuration mixings, are extensive. The list of references [11–21] represents only a tiny fraction of the full literature. In particular, the case of hard-core interactions, requiring resummations over infinite subsets of configurations to obtain effective interactions, defines a specific domain related to configuration mixings [22–25].

The standard view in matrix mechanics is that, since operators can be represented by matrices, one must balance between small matrices that are practical and larger ones that offer improved approximations at greater computational cost. It is also generally assumed that increasing the matrix size yields better convergence.

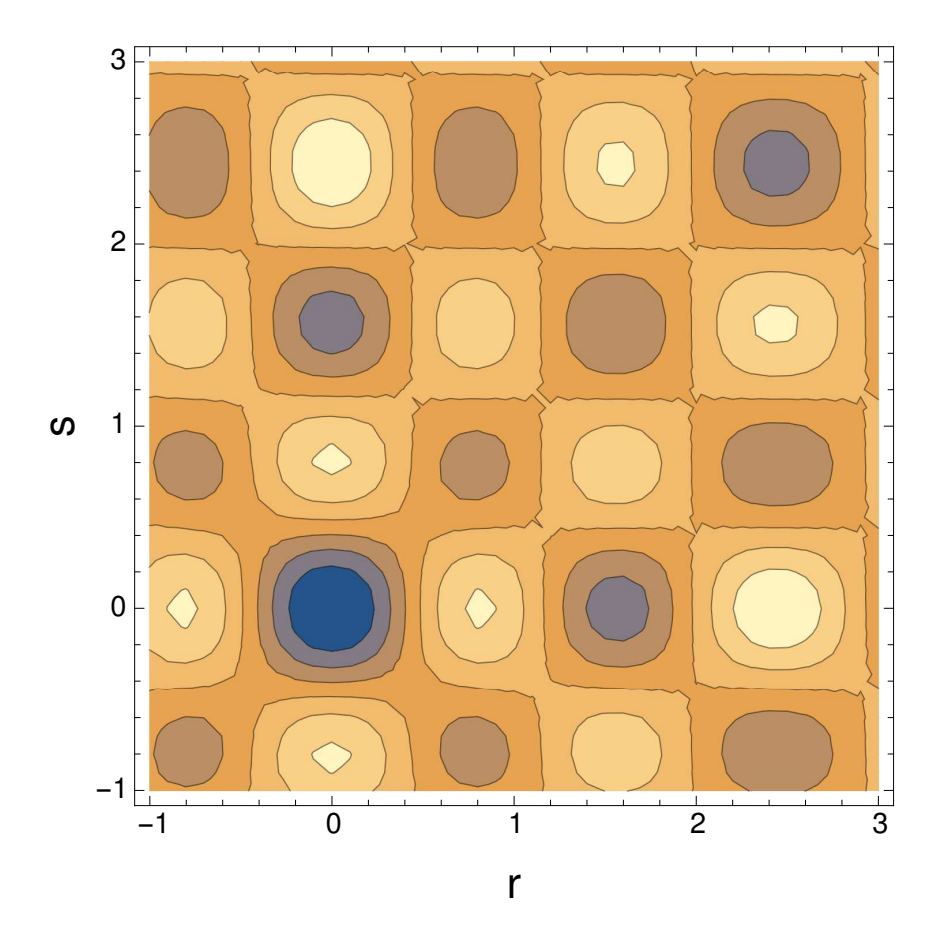


FIG. 25. As for Fig. 24, but for the effective potential W_{eff} .

Most matrix representations employ a discrete and finite orthonormal basis of configurations. (We are aware of the generator coordinate method [26–30], but it was not used here due to complications introduced by its norm kernel.) The essential point is that discrete orthogonal bases necessarily produce oscillating wave functions, which in turn generate interference effects in the matrix elements of operators and in resummations. These effects slow down the rate of convergence of the approximations.

We thus studied how elementary operators such as the identity, kinetic energy, harmonic potential, and toy potentials are represented in different bases. The analysis also included the Feshbach approach formulated in terms of complementary subspaces.

In the case where a suitable finite basis was chosen to truncate the Hilbert space to finite dimension, calculations using simple one-dimensional harmonic oscillators showed that convergence toward the exact operators (in the case of the δ function), or wave functions and their eigenvalues, is possible, but one cannot escape that convergence cannot be fast.

Yet, for the same finite number of basis states, a different expansion set of basis functions may yield better convergence. Such a choice may indeed be critical in cases where practical calculations are required.

When a splitting of the Hilbert space into two or three subspaces is necessary the issue is more serious. KA [1] identified a convergence problem when three subspaces, P, Q, and R are required and when only two of the three, P and Q, are used in calculations. The neglect of the third subspace may lead to serious convergences problems. In our case, where we investigated the diagonalisation of a toy Hamiltonian in the truncation of the included space, there is still a degree of locality, but the results indicated the non-locality that is introduced is due to the neglect of the third subspace. Further, the effective interaction becomes highly non-local, whereas the potential used in the toy Hamiltonian is clearly local.

One must take care in either scenario when taking results of calculations which are approximations to the exact physical problem. The question remains as to which approximation(s) are better in such usage. All told, we find that matrix approximations can be mathematically valid, but caution must be exercised concerning the choice of the approximation subspace and the rate of convergence.

Appendix A: Generalisations of the Christoffel-Darboux formula

We know that the idempotent kernel,

$$D_N(r,s) = \sum_{i=1}^{N} \varphi_i(r)\varphi_i(s)$$
(A1)

can be reduced to a simple, compact form,

$$D_{\text{cmpct}}(r,s) = \alpha(N)(s-r)^{-1} \left[\varphi_{N+1}(s) \varphi_N(r) - \varphi_{N+1}(r) \varphi_N(s) \right], \tag{A2}$$

where $\alpha(N) = \sqrt{\frac{N}{2}}$ for the harmonic oscillator basis. See [8] for the general case of orthogonal polynomials.

A similarly simpler form is available for the kernel

$$\mathcal{R}_{N}(r,s) = \sum_{i,j=1}^{N} \varphi_{i}(r) \langle i | r^{2} | j \rangle \varphi_{j}(s).$$
(A3)

From this we may write

$$r^{2}D_{N} = \sum_{i=1}^{N} r^{2}\varphi_{i}(r)\varphi_{i}(s)$$

$$= \sum_{i=1}^{N} \sum_{j=1}^{N+2} \varphi_{j}(r)\langle j | r^{2} | i \rangle \varphi_{i}(s). \tag{A4}$$

This is equivalent to

$$r^{2}D_{N} = \mathcal{R}_{N}(r,s) + \varphi_{N+1}(r) \frac{\sqrt{N(N+1)}}{2} \varphi_{N-1}(s) + \varphi_{N+2}(r) \frac{\sqrt{(N+1)(N+2)}}{2} \varphi_{N}(s), \quad (A5)$$

upon taking advantage of the symmetry and selection rules of the matrix element $\langle j | r^2 | i \rangle$. This provides $\mathcal{R}_N(r,s)$ in terms of r^2 times the compact form D_{empet} of D_N , and of a pair of corrective terms.

It is trivial to extend the present formalism to polynomials in r and d/dr. For instance, given $h = r^2 - d^2/dr^2$, the projected Hamiltonian $D_N h D_N$ benefits from a compact form,

$$D_N h D_N = r^2 D_{\text{cmpct}} - D_{\text{cmpct}}'', \tag{A6}$$

where the double prime denotes the second derivative with respect to r. No additional term is needed here, because the φ_i 's are eigenstates of h.

We recall here that such compact forms are of interest for the understanding of the spurious oscillations often introduced by truncations.

^[1] S. Karataglidis and K. Amos, Phys. Lett. B 660, 428 (2008).

^[2] T. F. Jordan, Linear operators for quantum mechanics (Dover Publishing, 2006).

^[3] A. D. Bain, Concepts Magn. Reson. Part A 28, 369 (2006).

^[4] N. Bebiano and J. da Providência, J. Math. Phys. 60 (2019).

^[5] R. L. Hall, J. Math. Phys. **25**, 2708 (1984).

^[6] R. G. Newton, J. Math. Phys. 1, 219 (1960).

^[7] B. G. Giraud, K. Kato, and A. Ohnishi, J. Phys. A 37, 11575 (2004).

^[8] B. Eynard, T. Kimura, and S. Ribault, "Random matrices," (2015), arXiv:1510.04430 [math-ph].

- [9] H. Feshbach, Ann. Phys. (N.Y.) 5, 357 (1958).
- [10] H. Feshbach, Ann. Phys. (N.Y.) 19, 287 (1962).
- [11] A. Prakash and N. Austern, Ann. Phys. **51**, 418 (1969).
- [12] J. B. McGrory, Phys. Rev. **160**, 915 (1967).
- [13] J. McGrory and B. H. Wildenthal, Ann. Rev. Nucl. Part. Sci. 30, 383 (1980).
- [14] J. Draayer, K. J. Weeks, and G. Rosensteel, Nucl. Phys. A 413, 215 (1984).
- [15] B. A. Brown and W. A. Richter, Phys. Rev. C **74**, 034315 (2006).
- [16] E. Terán and C. W. Johnson, Phys. Rev. C 73, 024303 (2006).
- [17] H. Grawe, in The Euroschool Lectures on Physics with Exotic Beams, Vol. I (Springer, 2004) p. 33.
- [18] E. Caurier, G. Martínez-Pinedo, F. Nowacki, A. Poves, and A. P. Zuker, Rev. Mod. Phys. 77, 427 (2005).
- [19] L. Coraggio, A. Covello, A. Gargano, N. Itaco, and T. T. S. Kuo, Prog. Part. Nucl. Phys. 62, 135 (2009).
- [20] Y. Kato, Y. Yamamoto, and T. Togashi, in J. Phys.: Conf. Series, Vol. 321 (IOP Publishing, 2011) p. 012006.
- [21] S. Karataglidis, K. Amos, P. R. Fraser, and L. Canton, A new development at the intersection of nuclear structure and reaction theory (Springer-Nature, Switzerland, 2019).
- [22] R. K. Nesbet, Phys. Rev. **109**, 1632 (1958).
- [23] A. Boutet de Monvel-Berthier, V. Georgescu, and A. Soffer, Rev. Math. Phys. 6, 515 (1994).
- [24] W. C. Haxton and T. Luu, Nucl. Phys. A **690**, 15c (2001).
- [25] S. R. Stroberg, H. Hergert, S. K. Bogner, and J. D. Holt, Ann. Rev. Nucl. Part. Sci. 69, 307 (2019).
- [26] J. J. Griffin and J. A. Wheeler, Phys. Rev. 108, 311 (1957).
- [27] Chun Wa Wong, Phys. Rep. 15, 283 (1975).
- [28] P. G. Reinhard and K. Goeke, Rep. Prog. Phys. 50, 1 (1987).
- [29] M. Verriere and D. Regnier, Front. Phys. 8, 233 (2020).
- [30] B. G. Giraud, J. C. Hocqenghem, and A. Lumbroso, Phys. Rev. C 7, 2274 (1973).